ELSEVIER

Journal of Nuclear Materials 250 (1997) 103–110

journal of nuclear materials

Helium bubbles in nickel annealed at $T > 0.7T_m$

V.N. Chernikov [a], H. Trinkaus [b,c], H. Ullmaier [b,c,*]

[a] *Institute of Physical Chemistry, Russian Academy of Sciences, Leninsky pr., 31, 117915 Moscow, Russian Federation*
[b] *Institut für Festkörperforschung, Forschungszentrum Jülich, D-52425 Jülich, Germany*
[c] *Association EURATOM-KFA, Jülich, Germany*

Received 31 July 1997; accepted 1 September 1997

Abstract

Helium-induced cavities in fusion materials are considered to be detrimental. Valuable information on He bubbles and on the basic mechanisms underlying their evolution is obtained by post-implantation annealing, subsequent to He implantation at about 300 K. For Ni and Cu, it has been shown that up to annealing temperatures $T_a \leq 0.7T_m$ (T_m is the melting point), highly overpressurized bubbles form in the volume and coarsen very slowly by migration and coalescence, whereas near vacancy sources the overpressure relaxes and the coarsening occurs rapidly by Ostwald ripening (OR) which leads to the appearance of small and large He cavities. Annealing of He loaded Ni at T_a from $0.72T_m$ to $0.92T_m$ leads to the formation of only one population of nearly equilibrium bubbles which is related to the recovery of the ability of dislocations to emit vacancies into their surroundings. The effective activation energy of the increase of the mean bubble radius was found to be 0.60 ± 0.02 eV, which is lower than that for the OR at lower temperatures (1.1 eV). Analysis shows that the mechanism covering the coarsening of He bubbles at very high temperatures is still OR, but limited by the rate of ledge nucleation on the bubble walls. © 1997 Elsevier Science B.V.

1. Introduction

Annealing of metals loaded with helium at low temperatures yields valuable information on the formation and coarsening mechanisms of gas bubbles. Such information is important for modelling the macroscopic property changes caused by helium in nuclear environments.

An analysis of experimental data on helium bubble coarsening in fcc Ni [1] together with theoretical considerations [2] resulted in the conclusion that the bubbles in the bulk can retain a considerable overpressure Δp (the difference between the actual pressure in a bubble of radius r_b and the equilibrium pressure, $2\gamma/r_b$, where γ is the specific surface energy) up to annealing temperatures T_a as high as 1200 K ($\approx 0.7T_m$, where T_m is the melting temperature) or even more. An important condition for this is that the implanted He concentration, c_{He}, is not too low (> 100 appm). Gas pressures exceeding the equilibrium values by about 3 GPa have indeed been measured directly by small angle scattering on bubbles in Ni [3] and FeCrNi [4]. Later the existence of overpressurized bubbles was also deduced for fcc Cu [5] loaded with helium and annealed, whereas in bcc W only near-equilibrium bubbles were found starting at $T_a \geq 0.4T_m$ [6].

According to [1,2,7] the main processes taking place in fcc Ni under post-implantation annealing in the range $(0.55–0.75)T_m$ can be summarized in short as follows (see the scheme in fig. 1 of Ref. [5]). First a high density of small overpressurized (primary) bubbles is formed throughout the whole volume of the matrix. The following bubble coarsening proceeds much faster near the outer surface and some grain boundaries (GBs) than within the grains. This leads to the formation of well-defined zones of large near-equilibrium (secondary) bubbles, where the gas-induced swelling is very high. The width of these high swelling regions increases with increasing annealing temperature T_a and time t_a [7]. The acceleration in the coarsening of small bubbles starts as a result of a gradual pressure

* Corresponding author. Tel.: +49-2461 613 160; fax: +49-2461 612410.

PII S0022-3115(97)00275-4

relaxation therein due to thermal vacancies supplied by vacancy sources, which leads in turn to the change of the coarsening mechanism. Vacancy sources are the outer surface and some GBs. The contribution of dislocations to vacancy production appears to be negligible. The main mechanism of rapid bubble coarsening is identified as Ostwald ripening (OR) occurring at moderate overpressure, whereas in the bulk, under the conditions of a lowered vacancy concentration (vacancy deficit), despite of a high mobility of vacancies, primary overpressurized

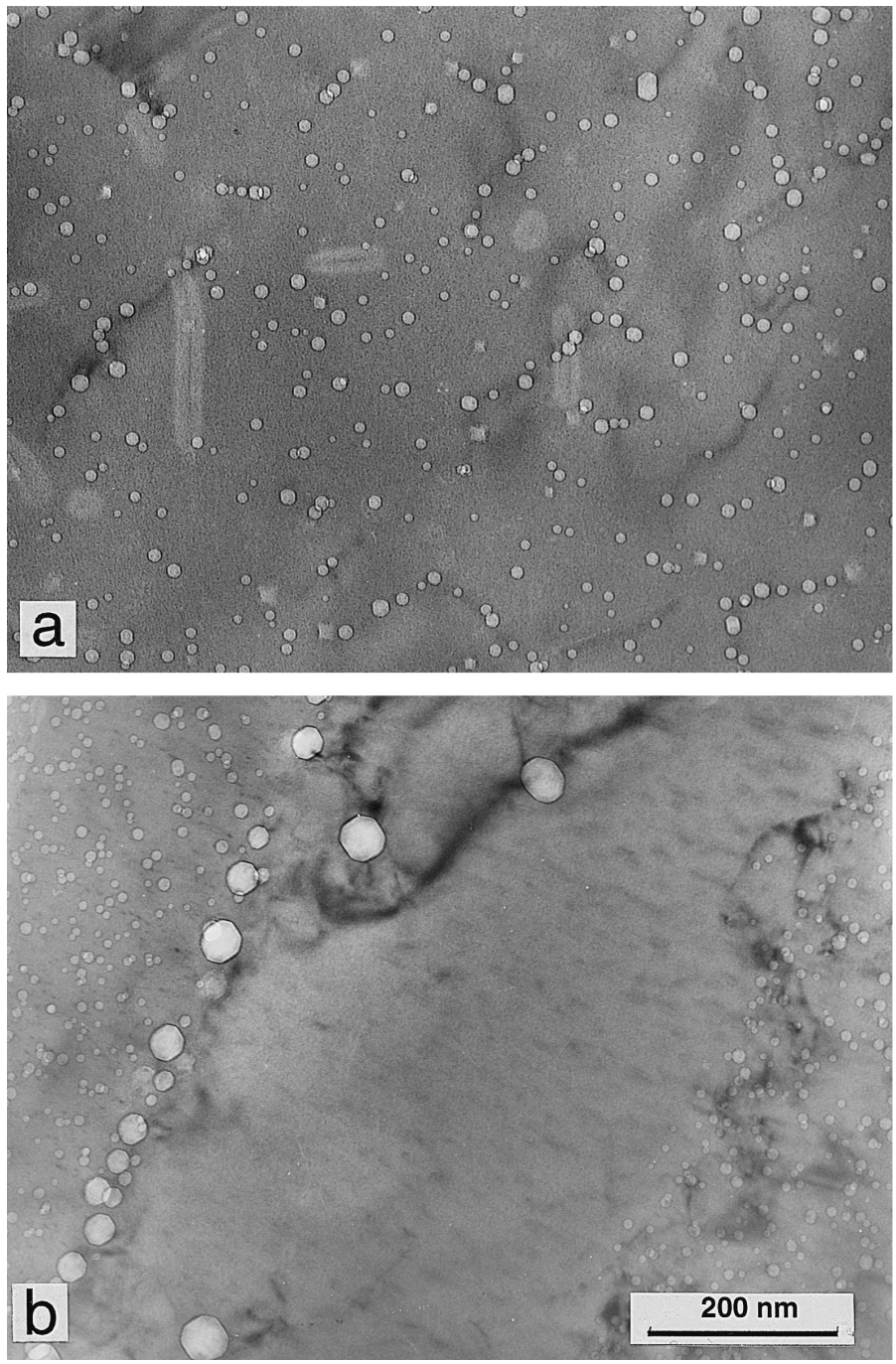

Fig. 1. Small helium bubbles in Ni implanted with 1400 appm He: (a) in the bulk of a grain after annealing at 1600 K, and (b) near a migrating GB sweeping small He bubbles out from one (right) of neighbouring grains after annealing at 1500 K. Annealing time is 1 h.

bubbles coarsen slowly by migration and coalescence (MC).

It seems to be clear that at these temperatures the main reason for a *temporary* existence of overpressurized bubbles is the *inability of dislocations in the fcc metals Ni and Cu to emit vacancies into the surroundings* (dislocation density ρ_d of 10^{14}–10^{15} m^{-2}). This effect was already pointed out by Barnes [8] who investigated He implanted and annealed Cu as early as in 1960. In Ref. [5] this phenomenon in both fcc Cu and Ni was attributed to the accumulation of some quantities of He atoms (up to tens of appm) within edge dislocation cores which was assumed to increase substantially both the binding energy of He atoms to a dislocation and the activation energy for vacancy emission by a dislocation. In the same work [5] deviations of the temperature dependence of the mean bubble radius $\bar{r}_b(T)$ from a simple Arrhenius behaviour were noticed around $0.7T_m$, and it was concluded that such a behaviour could be a first indication for a loss of binding of He atoms to dislocation cores and consequently vacancy emission by dislocations. So, it seemed to be interesting to study the temperature dependence of the mean bubble radius of primary bubbles in Cu or Ni in the temperature range between $T_r \cong 0.7T_m$ and T_m.

The aim of the present work was to investigate in detail the temperature dependence of the mean bubble radius, $\bar{r}_b$, gas-induced swelling, $\bar{S}$, and dislocation density, $\bar{\rho}_d$, under conditions of isochronal annealing in the T_a range from 0.72 to $0.93T_m$, for checking the expectations quoted above and modelling the relevant processes.

2. Experimental

Nickel with 99.995% purity was used for the preparation of foil samples with a thickness of 90 μm. Homogeneous helium implantation into these samples at room temperature was achieved by continuously varying the energy of the α-beam of the FZ-Compact Cyclotron between 0 and 28 MeV (for details see Ref. [1]). The implantation resulted in a total nominal helium concentration of about 1400 appm coupled with displacement damage in the order of 0.15 dpa. From the implanted samples discs of 3 mm diameter were punched out and annealed in UHV at $T_a = 1400$, 1420, 1500 and 1600 K, respectively, for 0.5 or 1.0 h. Long-term isothermal annealings cited in the discussion were performed in vacuum better than 10^{-4} Pa at 998 K for the times up to 1000 h. The annealed specimens were thinned from both sides using jet electropolishing to obtain TEM specimens.

The specimens were investigated in a Philips EM-430 microscope operated at 300 kV. Average bubble radii $\bar{r}_b$ were determined from histograms obtained with a particle size analyser Zeiss TGA-10. The mean radii of small (see below) bubbles formed during different annealing times were normalized to the annealing time $t_a = 1$ h on the basis of isothermal annealing data. For the evaluation of bubble densities, c_b, the foil thickness was determined by analysing stereomicrographs. The concentration of helium accumulated in bubbles, c^b_{He}, was estimated using Trinkaus equation of state for helium [9]. Due to the fact that c^b_{He} values varied slightly in different samples, the calculated absolute values of the gas-induced swelling, S^{abs}, were normalized to a concentration $c^b_{He} = 1000$ appm: $S^n = S^{abs} \times 1000/c^b_{He}$(appm). The dislocation density ρ_d was determined using the intersection analysis [10].

3. Experimental results

In specimens subjected to annealing at $T_a \geq 0.72T_m \equiv T_r$ we failed to notice any zones with large bubbles near GBs which are usually observed at lower annealing temperatures and which were described and discussed in detail in Refs. [1,7,11]. The bubbles in the matrix were relatively small with sizes somewhat larger, but of the same order of magnitude as the matrix bubbles produced at $T_a \leq T_r$. A part of these bubbles was coupled with dislocations. Large bubbles also exist in the high temperature specimens, but they are observed not in zones adjacent to GBs, but directly on GBs evidently as a result of GB migration and sweeping small bubbles out from the interior of grains. The latter effect is clearly seen in Fig. 1, where a GB is shown which has swept small He bubbles from the bulk of the right grain resulting in the formation of larger bubbles on the GB itself. All bubbles appear to be clearly faceted.

The $\bar{r}_b$ versus T_a data in the range of $(0.72–0.93)T_m$ are presented (branch 3) in Fig. 2 together with our earlier data on $\bar{r}_b(T_a)$ for primary and secondary bubbles taken

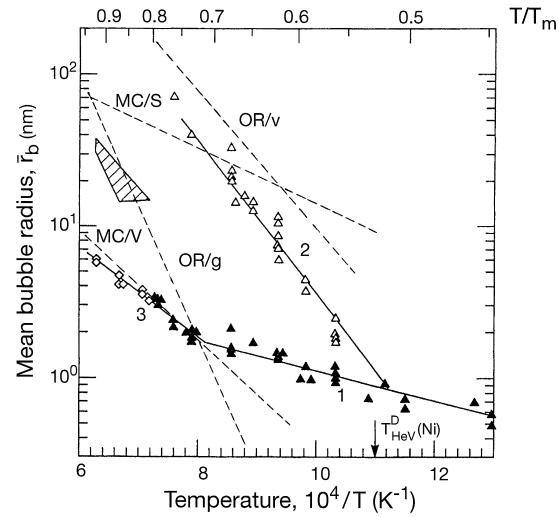

Fig. 2. Summary plot of the mean radius, $\bar{r}_b$, of primary (1) and secondary (2) bubbles, and bubbles formed at $T_a \geq 0.72T_m$ (3) in helium loded Ni as a function of annealing temperature T. Hatched area comprises radii of bubbles found and formed on GBs due to their migration. (◇) Present work; (△, ▲) from Refs. [1,7]. Dotted lines are theoretical expectations (see text).

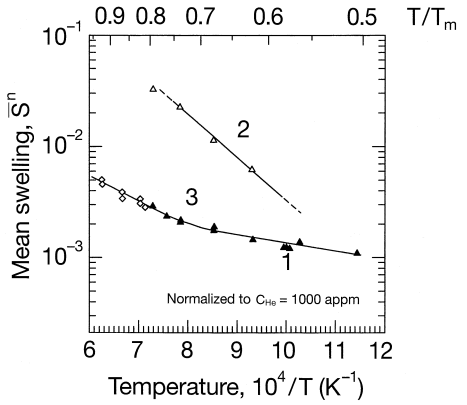

Fig. 3. Temperature dependence of the normalized (to 1000 appm He) mean gas-induced swelling, $\bar{S}^n$, in helium loaded Ni due to primary (1) and secondary (2) bubbles, and small bubbles formed at $T_a \geq 0.72T_m$. (◇) Present work; (△, ▲) points calculated from data in Refs. [1,7].

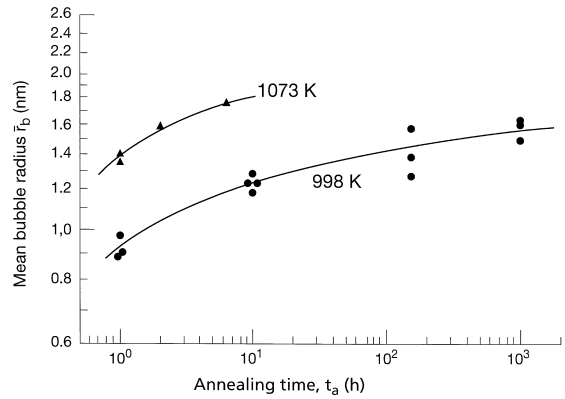

Fig. 5. Time dependencies of the mean bubble radius during isothermal annealing at 1073 K [21] and 998 K [22].

from Ref. [7] and denoted by filled (branch 1) and open (branch 2) triangles, respectively. The lines fitting these data branches are given by the following expressions:

branch 1: $r_b = 11\ \text{nm} \times \exp(-2250/T)$,

branch 2: $r_b = 10^6\ \text{nm} \times \exp(-12500/T)$, and

branch 3: $r_b = 4 \times 10^2\ \text{nm} \times \exp(-6700/T)$, or

$$r_b = 1.2 \times 10^{-2}\ \text{nm/K} \times (T - 1120\ \text{K}).$$

It is clearly seen that starting from $T_a = T_r \cong 0.72T_m$ the effective activation energy of coarsening changes to $E_r = 0.60 \pm 0.02$ eV which is higher than E_r of the bubble coarsening by MC (0.25 eV, branch 1 in Fig. 2), but lower than that attributed to OR ($E_r = 1.1$ eV, branch 2). The hatched tetragon in Fig. 2 denotes the range of mean $\bar{r}_b$ values (15–40 nm) for large bubbles found directly on GBs. But even these values are significantly lower than the estimated radii of secondary bubbles (branch 2) provided they could appear, but, as mentioned, they do not develop at all at $T_a > T_r$.

Fig. 3 presents the mean gas-induced swelling $\bar{S}^n$ in regions of primary (branch 1) and secondary (branch 2) bubbles formed at $T_a < T_r$ and for small bubbles (branch 3) developed at $T_a > T_r$. The swelling data related to GB bubbles formed at $T_a > T_r$ are not presented. Similar to the behaviour of $\bar{r}_b$, the slope of the swelling dependence $\bar{S}^n(T_a)$ changes at $T_a > T_r$. It is worth noting that $\bar{S}^n$ for the primary bubbles (branch 1 in Fig. 3) changes very weakly, but does not remain constant as it was assumed in a first approximation in our previous theoretical considerations [1,2,7].

Data on the dislocation density $\rho_d(T)$ in zones of Ni with small bubbles (corresponding to branches 1 and 3 in Fig. 2) are given in Fig. 4. The data show a tendency of the dislocation density to decrease with increasing T_a for $T_a > T_r$, which seems to be correlated with the change in the bubble coarsening rate found in this temperature range. In this connection it should be recalled that in the temperature range of interest here, possible dislocation densities in pure Ni (minimum recrystallization temperature $\cong 873$ K $= 0.51T_m$ [12]) are orders of magnitude smaller than the values in Fig. 4, including those at $T_a = 0.93T_m$. This demonstrates the high efficiency of helium bubbles for suppressing recovery and recrystallization. Results of long-term isothermal annealings are presented in Fig. 5.

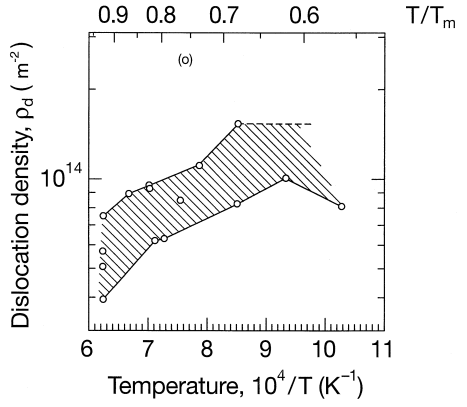

Fig. 4. Dislocation density, ρ_d, in areas of Ni with small helium bubbles having radii denoted in Fig. 2 by branches 1 and 3.

4. Discussion

The main features in the annealing behaviour of bubbles in He implanted Ni above $T_r = 0.72T_m$ to be discussed in the following are: (1) the disappearance of enhanced coarsening in regions adjacent to the outer surface and GBs (the appearance of enlarged bubbles directly on GBs

is attributed to sweeping of smaller bubbles during GB migration), (2) the change in the temperature dependence of the remaining small bubble population and, particularly, the increase in the apparent activation energies of the mean bubble size, volume density and swelling.

According to our interpretation [1], at temperatures *below* T_r the difference between the bubble populations in the bulk and near planar vacancy sources is due to differences in the pressure within the two types of bubbles. In the bulk, the high overpressure in the bubbles cannot relax since the vacancy emission by the existing dislocations is blocked by a dense row of He atoms in their cores [5], and this overpressure suppresses coarsening by OR, but allows coarsening by MC even though only at a strongly reduced rate. In regions adjacent to efficient vacancy sources, on the other hand, the overpressure is partially relaxed to moderate values at which OR occurs most effectively and dominates over MC. The spatial homogeneity of approximately equisized bubbles *above* T_r (except of those at migrating GBs) indicates that the pressure in bubbles which governs their coarsening is approximately the same everywhere including zones near planar vacancy sources. Near the latter this pressure is equilibrated with the surface tension already at $T_a < T_r$, and the more so at $T_a > T_r$. Consequently, at $T_a > T_r$ the pressure in all the bubbles is close to its equilibrium value $p = 2\gamma/\bar{r}_b$.

At such high temperatures, (edge) dislocations can no longer retain He atoms in their cores and become efficient vacancy sources in addition to the outer surface and GBs. This interpretation is confirmed by the observed partial recovery of the dislocation density by about a factor of 2 as shown in Fig. 4 which requires both glide and climb, i.e. the emission and absorption of vacancies. Thus, the difference between bulk regions and regions close to planar vacancy sources is removed. Under the now global vacancy supply (at dislocation densities somewhat below 10^{14} m^{-2}), the initial overpressure in small bubbles as well as the reduced vacancy concentration in their environment will quickly relax to their thermal equilibrium values. Estimates show that the decrease in the dislocation density by about 5×10^{13} m^{-2} is sufficient to provide the vacancies required for bubble relaxation. Obviously, this process proceeds so fast that the time interval at which the rate of OR is maximum is passed before substantial bubble coarsening could occur by this mechanism. Consequently no zones of enhanced coarsening are found adjacent to planar vacancy sources. A stronger decrease of the dislocation density which could be expected at $T_a > T_r = 0.72T_m$ does not take place due to their pinning on numerous and still relatively small bubbles.

In the following we make an attempt to identify the mechanism responsible for bubble coarsening above $T_r \cong$ 1250 K. According to our preceding discussion, we assume that the helium pressure within the bubbles is close to its equilibrium value $p = 2\gamma/\bar{r}_b$. In addition, for the corresponding pressure level (1 GPa for $\gamma = 2$ N m^{-1} and $r_b = 4$ nm) and the high temperatures considered the gas may be assumed to obey the ideal gas law.

We consider the two main coarsening mechanisms: MC and OR. For ideal gas behaviour, the increase in the mean bubble radius due to MC may be approximately described by [1,2]

$$\mathrm{d}\bar{r}_b/\mathrm{d}t \cong \tfrac{3}{2} D_b c_{He} kT/\gamma\Omega, \tag{1}$$

where D_b is the bubble diffusion coefficient, kT is the thermal energy and Ω is the atomic volume of the matrix. D_b depends on the mechanism controlling bubble migration. For bubble migration controlled by surface diffusion, it is given by [2,13]

$$D_b \cong 3\Omega^{4/3} D_S/2\pi r_b^4, \tag{2}$$

where D_S is the surface self-diffusion coefficient. For volume diffusion controlled bubble migration, D_b is given by [13]

$$D_b \cong 3\Omega D_V/4\pi r_b^3, \tag{3}$$

where D_V is the volume self-diffusion coefficient. Explicit time dependencies, $r_b(t)$, are obtained by integrating Eq. (1) with using Eqs. (2) and (3) yielding $r_b^5 \propto D_S t$ in the first and $r_b^4 \propto D_V t$ in the second case, respectively.

OR of gas bubbles may be gas dissociation or vacancy dissociation controlled depending on which process is more difficult [2]. In the former case, the mean radius of bubbles containing ideal gas increases with time as [14]

$$\mathrm{d}\bar{r}_b^2/\mathrm{d}t \approx kTD_{He}K_{He}, \tag{4}$$

where D_{He} is the He diffusion coefficient and K_{He} is the He solubility coefficient of Sieverts' law. The activation energy of the He permeation coefficient $P_{He} = D_{He}K_{He}$ is identical with the energy for the dissociation of a He atom from a bubble into the matrix. In the case of vacancy dissociation controlled OR, the mean bubble radius increases with time according to the classical Lifshitz–Slyozov–Wagner theory as [2,15,16]

$$\mathrm{d}\bar{r}_b^3/\mathrm{d}t = \tfrac{8}{9}(\gamma\Omega/kT) D_V. \tag{5}$$

According to Eq. (1) together with Eqs. (2)–(5) the apparent activation energy of the $\bar{r}_b$ evolution, E_r, reflects the activation energy of the diffusion process controlling MC and/or of the dissociation process controlling OR, respectively. According to Eq. (1) together with Eqs. (2) and (3), $E_S = 5E_r$ and $E_V = 4E_r$, respectively, in the case of surface and volume diffusion controlled bubble MC (where E_S and E_V are the surface and volume diffusion activation energies, respectively); whereas, according to Eqs. (4) and (5), in the case of He atom and vacancy dissociation controlled OR, $E_{He}^{diss} = 2E_r$ and $E_V^{diss} = 3E_r$, respectively (where E_{He}^{diss} and $E_V^{diss} \cong E_V$ are the activation energies of He atom and vacancy dissociation from a bubble, respectively; the latter is approximately equal to the activation energy of the self-diffusion, E_V). So, the value of an apparent activation energy $E_r = 0.6$ eV de-

duced from our experimental data would result in the following relations: $E_S = 3$ eV, $E_V = 2.4$ eV, $E_{He}^{diss} = 1.2$ eV, or $E_V^{diss} = 1.8$ eV, respectively. A value of 3 eV is clearly above the range expected for E_S of Ni (< 2 eV [17]), and the values of 1.2 and 1.8 eV are, respectively, considerably below the ranges expected for E_{He}^{diss} and $E_V^{diss} \cong E_V$ of the same metal ($E_{He}^{diss} \geq 3$ eV [2,18], $E_V = 2.9$ eV [18]). On the other hand, a value of 2.4 eV is not too far from the value of $E_V = 2.9$ eV.

Additional information may be expected from a comparison of the absolute values of bubble radii observed in our experiments with those expected according to Eqs. (1)–(5). In Fig. 2, we have included the $\bar{r}_b(T)$ dependencies corresponding to MC controlled by surface and volume diffusion, and to OR controlled by He atom and vacancy dissociation, assuming $c_{He} = 10^{-3}$, $\gamma = 2$ N m^{-1}, $\Omega = 11 \times 10^{-30}$ m^3, $D_S = 2.5 \times 10^{-2}$(m^2 s^{-1})exp(-1.8 eV$/kT$) [17], $D_V = 10^{-4}$(m^2 s^{-1})exp(-2.9 eV$/kT$) [18], $E_{He}^{diss} = 3.5$ eV [2,18], $t = 1$ h and the statistical mechanics expression for K_{He} [19,20]. The analytical expressions for curves fitting theoretical $r_b(T)$ dependencies and plotted in Fig. 2 as dotted lines are as follows:

- for MC controlled by the surface diffusion (MC/S): $r_b = 945$ nm $\times$ exp($-4200/T$),
- for MC controlled by the volume diffusion (MC/V): $r_b = 1500$ nm $\times$ exp($-8400/T$),
- for OR controlled by the He dissociation (OR/g): $r_b = 2 \times 10^7$ nm $\times$ exp($-20300/T$) and
- for OR controlled by the vacancy dissociation (OR/v): $r_b = 7 \times 10^5$ nm $\times$ exp($-11200/T$).

It is appropriate to remember that analytical expressions for the theoretical (solid) lines fitting the branches 1 and 2 in Fig. 2 were derived in Ref. [1] taking into account the overpressure available in both primary and secondary bubbles.

The lines for both types of OR as well as the line for MC by surface diffusion are significantly above the experimental data, whereas the line for MC by volume diffusion seems to fit these data quite well. It is rather tempting to conclude from this that the mechanism underlying bubble coarsening in the high temperature range would be MC controlled by volume diffusion.

Drawing this conclusion, we would have to explain, however, for which reason the apparently more efficient processes of common OR and MC by surface diffusion are impeded. It should be noted that the partial rates of OR due to He atom and vacancy dissociation superimpose reciprocally as in series connections [2], whereas the total rate of OR and the rates of the different MC processes superimpose linearly as in shunt connections. Since the bubbles observed at high temperatures are clearly faceted, the most likely explanation for the strong retardation of bubble coarsening is the necessity of ledge nucleation on planar bubble facets [13]. This is associated with a strong slowing down of the coarsening rate, especially, with increasing bubble size. Such an effect is indeed observed at $r_b > 1$ nm in long-term isothermal annealing experiments (Fig. 5, see below).

Below, it will be shown that a deeper insight into the phenomenology of bubble coarsening limited by ledge nucleation brings to light other criteria for the feasibility of different coarsening mechanisms.

First of all, in spite of the fact that the ledge nucleation is commonly considered to limit MC [13], it is also a necessary step in growth and shrinkage of bubbles which coarsen by OR [23]. Considering ledge nucleation to limit coarsening we may assume He exchange between the bubbles to become faster than growth and shrinkage of the bubbles meaning that OR occurs then at virtually constant He pressure. In this case, a useful approximation to account for ledge nucleation in MC and OR is to simply multiply the diffusion constants D_b and D_V in Eqs. (1)–(5), respectively, with a Boltzmann factor containing the energy of ledge formation, $\exp(-\varepsilon l/kT)$, where ε is the specific ledge energy and l is the ledge length scaling linearly with the bubble size, say as $l = \alpha r_b$ (α is the geometrical factor). Approximate integration of the correspondingly modified Eqs. (1)–(5) yields then expressions of the form [23]

$$\alpha \varepsilon \bar{r}_b = kT \ln(\nu t) - E, \tag{6}$$

where ν is a (r_b dependent) frequency summarizing the parameters in Eqs. (1)–(3) and (5) and $E = E_S$ or E_V is the activation energy of the diffusion process responsible for ledge nucleation.

According to Eq. (6), $\bar{r}_b$ would show an approximately linear T-dependence rather than Arrhenius behaviour. In fact, a linear fit to our $\bar{r}_b$ data in the high temperature range is as good as an Arrhenius one (see Section 3). Besides, the t-dependence of r_b would be approximately logarithmic which is confirmed by our long-term isothermal annealing data (Fig. 5).

A comparison of Eq. (6) with experimental data may be used to identify the basic coarsening mechanism limited by ledge nucleation. Formally (allowing $\bar{r}_b \to 0$) Eq. (6) defines an apparent lower temperature limit, T_l, at which ledge nucleation controlled bubble coarsening would vanish completely

$$T_l = E\left[k \ln(\nu\tau)\right]^{-1}. \tag{7}$$

Using the parameter values quoted above we estimate $T_l \cong 750$ and 1200 K for ledge nucleation limited MC by surface and volume diffusion, respectively, and $T_l \cong 950$ K for ledge nucleation limited OR. Extrapolating our high temperature $\bar{r}_b$ data to zero we find $T_l \cong 1120$ K which is between the estimated T_l values for ledge nucleation limited OR and MC by volume diffusion. On the basis of T_l values we may rule out ledge nucleation limited MC by surface diffusion where the theoretical T_l value is far below the experimental value. We favour ledge nucleation limited OR as the mechanism controlling coarsening of bubbles at high temperatures since this is the fastest pro-

cess in the absence of ledge nucleation (upper line in Fig. 2). The good agreement between MC by volume diffusion and experimental data must be considered to be accidental. Thus, we conclude that the mechanism controlling He bubble coarsening in Ni at high temperatures is certainly a ledge nucleation limited process and this process is most likely OR.

Additional information is provided by the linear temperature coefficient of $\bar{r}_b(T)$, and the derivative $\partial\bar{r}_b/\partial T$, which is about 1.2×10^{-2} nm K^{-1} according to our experimental data. Using this value together with the experimental value of 1120 K for T_l and assuming $\alpha\approx1$ ($l\approx r_b$) in Eq. (6) we can estimate the specific ledge energy, ε, as

$$\varepsilon = E_V\left(T_l\,\partial r_b/\partial T\right)^{-1} \cong 3.4\times10^{-11}\ \mathrm{J\ m^{-1}}, \qquad (8)$$

which is in the range expected for specific ledge energies [13].

We should not keep secret that our conclusions pose another question to be answered: Why should OR of equilibrium bubbles *above* T_r be ledge nucleation limited whereas OR of moderately overpressurized bubbles *below* T_r not? Our experimental observations show that the secondary bubbles below T_r are not as clearly faceted as the bubbles throughout the volume observed above T_r. So, the ledge nucleation might indeed not be so important in this case. A fully satisfying answer to this question is beyond the scope of this paper but one remark concerning the inefficiency of ledge nucleation in OR of moderately overpressurized (secondary) bubbles is in order here. For the growing part of the bubbles (large bubbles) the energetic barrier against ledge nucleation is reduced or even removed by the action of the overpressure [1,2], whereas for the shrinking part of the bubbles (small bubbles) this barrier is low because of the short ledge length. Details of this explanation will be presented elsewhere [23].

5. Summary and conclusions

The enhancement of bubble coarsening in the vicinity of vacancy sources does not occur in He implanted Ni within an interval of annealing temperatures, T_a, from $0.72T_m$ to $0.92T_m$, which results in the formation of only one main population of nearly equilibrium He bubbles (anomalously large bubbles on GBs formed due to GB migration and sweeping of small bubbles are of less interest here and are not discussed). This is in contrast to the T_a range of $(0.55–0.70)T_m$ where two different kinds of bubbles, including highly overpressurized ones, are observed [1]. The change in the bubble evolution is attributed to the recovery of the ability of dislocations to emit vacancies into their surroundings.

The overall evolution of these high temperature bubbles accelerates with increasing temperature, but at a slower rate than it could be expected in the case of OR characteristic for $T_a < 0.7T_m$. The effective activation energy of the $\bar{r}_b(T)$ dependence, E_r, is 0.60 ± 0.02 eV, which is lower than that for OR at lower temperatures ($E_r\cong1.1$ eV).

The experimental data on the mean bubble radius, $\bar{r}_b(T)$, versus the annealing temperature within the temperature interval $T_a > 0.72T_m$ were compared with theoretical expectations for different coarsening processes of nearly equilibrium bubbles: migration and coalescence controlled by surface diffusion (MC/S) and by volume diffusion (MC/V) and Ostwald ripening controlled by vacancy dissociation (OR/v) and by He atom dissociation (OR/g). It was tempting to identify the coarsening process in question as MC/V, but a deeper insight into the phenomenology of bubble coarsening limited by ledge nucleation made us to conclude that the mechanism controlling He bubble coarsening in Ni at high temperatures is certainly a ledge nucleation limited process, and this process is most likely OR.

For the first time, experimental data are presented on the evolution of helium bubbles in Ni for the full range of post-implantation annealing temperatures. To our knowledge, such data have not been reported before for any metal.

There are indications that at $T_a > (0.70–0.75)T_m$ the formation of nearly equilibrium bubbles which behave differently compared to those at $T_a < 0.7T_m$ occurs also in other metals, and in particular, in fcc Cu [5] and hcp Be [24].

Acknowledgements

The work of V.N.Ch. in Moscow was supported in part by the Grant No. 96-03-33953 of the Russian Foundation of Fundamental Research.

References

[1] V.N. Chernikov, H. Trinkaus, P. Jung, H. Ullmaier, J. Nucl. Mater. 170 (1990) 31.
[2] H. Trinkaus, Scr. Metall. 23 (1990) 1773.
[3] L. Qiang, W. Kesternich, H. Schröder, D. Schwahn, H. Ullmaier, Acta Metall. Mater. 38 (1990) 2383.
[4] F. Carsughi, W. Kesternich, D. Schwahn, H. Ullmaier, J. Nucl. Mater. 191–194 (1992) 1284.
[5] V.N. Chernikov, J. Nucl. Mater. 195 (1992) 29.
[6] V.N. Chernikov, Ju.V. Lakhotkin, H. Ullmaier, H. Trinkaus, P. Jung, H.J. Bierfeld, J. Nucl. Mater. 212–215 (1994) 375.
[7] V.N. Chernikov, P.R. Kazansky, H. Trinkaus, P. Jung, H. Ullmaier, in: Fundamental Aspects of Inert Gases in Solids, Proc. NATO Adv. Res. Workshop, Bonas, France, Plenum, London, 1991, p. 329.
[8] R.S. Barnes, Philos. Mag. 5 (1960) 635.
[9] H. Trinkaus, Radiat. Eff. 78 (1983) 189.

[10] P.B. Hirsch, A. Howie, R.B. Nicholson, D.W. Pashley, M.J. Whelan, Electron Microscopy of Thin Crystals, Butterworth, London, 1965, p. 422.
[11] V.N. Chernikov, P.R. Kazansky, J. Nucl. Mater. 172 (1990) 155.
[12] R. Brick, A. Pense, R. Gordon, Structure and Properties of Engineering Materials, McGraw-Hill, New York, 1977, p. 83.
[13] P.J. Goodhew, S.K. Tyler, Proc. Roy. Soc. London A 377 (1981) 151.
[14] A.J. Markworth, Metall. Trans. 4 (1973) 2651.
[15] I.M. Lifshitz, V.V. Slyozov, J. Phys. Chem. Solids 19 (1961) 35.
[16] C. Wagner, Z. Elekrochem. 65 (1961) 581.
[17] G. Neumann, G.M. Neumann, in: F.H. Wöhlbier (Ed.), Surface Self-Diffusion of Metals, No. 1, Bay Village, Solothurn, 1972.
[18] O. Madelung (Ed.), Landolt–Börnstein, N.S. III 25, Springer, Berlin, 1991, p. 243.
[19] G.W. Greenwood, A. Boltax, J. Nucl. Mater. 5 (1962) 234.
[20] K.C. Russel, Acta Metall. 20 (1972) 899.
[21] W. Kesternich, D. Schwahn, H. Ullmaier, Scr. Metall. 18 (1984) 1011.
[22] V.N. Chernikov, H. Ullmaier, unpublished data.
[23] H. Trinkaus, to be published.
[24] V.N. Chernikov, H. Ullmaier, A.P. Zakharov, Gas bubbles in beryllium implanted with He ions at temperatures ≤ 700 K and after post-implantation annealing, Proc. ICFRM-8, Oct. 26–31, 1997, Sendai, Japan, J. Nucl. Mater., to be published.